Available online at www.sciencedirect.com
ScienceDirect
Atmospheric Environment 41 (2007) 9341–9352
ATMOSPHERIC ENVIRONMENT
www.elsevier.com/locate/atmosenv

Large outdoor chamber experiments and computer simulations: (I) Secondary organic aerosol formation from the oxidation of a mixture of d-limonene and α-pinene

Qianfeng Li[1], Di Hu, Sirakarn Leungsakul, Richard M. Kamens*

Department of Environmental Sciences and Engineering, The University of North Carolina at Chapel Hill, Chapel Hill, NC 27599-7431, USA

Received 29 January 2007; received in revised form 19 August 2007; accepted 4 September 2007

Abstract

This work merges kinetic models for α-pinene and d-limonene which were individually developed to predict secondary organic aerosol (SOA) formation from these compounds. Three major changes in the d-limonene and α-pinene combined mechanism were made. First, radical–radical reactions were integrated so that radicals formed from both individual mechanisms all reacted with each other. Second, all SOA model species from both compounds were used to calculate semi-volatile partitioning for new semi-volatiles formed in the gas phase. Third particle phase reactions for particle phase α-pinene and d-limonene aldehydes, carboxylic acids, etc. were integrated. Experiments with mixtures of α-pinene and d-limonene, nitric oxide (NO), nitrogen dioxide (NO_2), and diurnal natural sunlight were carried out in a dual 270 m^3 outdoor Teflon film chamber located in Pittsboro, NC. The model closely simulated the behavior and timing for α-pinene, d-limonene, NO, NO_2, O_3 and SOA. Model sensitivities were tested with respect to effects of d-limonene/α-pinene ratios, initial hydrocarbon to NO_x (HC_0/NO_x) ratios, temperature, and light intensity. The results showed that SOA yield (Y_{SOA}) was very sensitive to initial d-limonene/α-pinene ratio and temperature. The model was also used to simulate remote atmospheric SOA conditions that hypothetically could result from diurnal emissions of α-pinene, d-limonene and NO_x. We observed that the volatility of the simulated SOA material on the aging aerosol decreased with time, and this was consistent with chamber observations. Of additional importance was that our simulation did not show a loss of SOA during the daytime and this was consistent with observed measurements.

Keywords: d-Limonene; α-Pinene; Kinetics mechanism; Model simulation; SOA

1. Introduction

Recently, gas-particle partitioning (G/P) theory (Odum et al., 1996; Pankow, 1994) has been used to represent secondary organic aerosol (SOA) formation in a number of studies (Dechapanya et al., 2003; Kamens et al., 1999; Kamens and Jaoui, 2001; Leungsakul et al., 2005b; Takekawa et al., 2003). In addition to G/P, heterogeneous reactions are proposed to take place in the particle phase

*Corresponding author. Tel.: +1 919 966 5452; fax: +1 919 966 7911.
E-mail addresses: qli5@ncsu.edu (Q. Li), kamens@unc.edu (R.M. Kamens).
[1]Present address: Air Quality Engineering, Biological & Agricultural Engineering Department, North Carolina State University, Raleigh, NC 27695, USA.

1352-2310/$ - see front matter © 2007 Elsevier Ltd. All rights reserved.
doi:10.1016/j.atmosenv.2007.09.017

(Gao et al., 2004b; Jang et al., 2002; Kalberer et al., 2004; Tolocka et al., 2004). This further aids in the uptake via G/P of volatile compounds and the formation of large molecules within the aerosol. Oligomers formed by particle phase reactions have been observed from individual systems of α-pinene, 1,3,5-trimethylbenzene and glyoxal (Gao et al., 2004b; Kalberer et al., 2004; Liggio et al., 2005a, b; Tolocka et al., 2004).

The first aim of the present study was to update the kinetic models of α-pinene (Kamens et al., 1999; Kamens and Jaoui, 2001) and d-limonene (Leungsakul et al., 2005a, b), which were individually developed to predict SOA formation. Three major changes in the d-limonene and α-pinene combined mechanism were made. First, radical–radical reactions were integrated so that radicals formed from both individual mechanisms all reacted with each other. Second, all SOA species from both compounds were used to calculate semi-volatile partitioning for new semi-volatiles formed in the gas phase. The third was the incorporation of particle phase reactions for particle phase α-pinene and d-limonene aldehydes, carboxylic acids, etc.

The secondary aim was to evaluate the merged mechanism with previous individual α-pinene only and d-limonene only experiments, and with a new series of α-pinene and d-limonene mixture experiments that had different initial conditions. To our knowledge this is the first mixture terpene dataset that has been generated to evaluate SOA model performance. In addition, these experiments push the lower concentration boundary of experiments of this type. It is shown that it is possible to integrate individual semi-explicit mechanisms into a combined mechanism and fit terpene binary mixture experiments.

Model sensitivity was tested and discussed with respect to effects of d-limonene/α-pinene ratios, HC_0/NO_x ratios, temperature and light intensity. These results allowed us to identify the most important parameters and processes, and recommend experiments needed to improved models of SOA formation from realistic mixtures. Also, the model was used to simulate more realistic remote atmospheric SOA conditions that hypothetically could result from diurnal emissions of α-pinene, d-limonene and NO_x.

2. Experimental section

New experiments were carried out in the UNC 270 m^3 dual outdoor aerosol smog chambers located in Pittsboro, NC. Chamber descriptions are presented elsewhere (Lee et al., 2004; Leungsakul et al., 2005b). Briefly, each chamber half was designated as either north or south. Prior to each experiment, the chambers were continuously flushed with clean rural air for 4–8 h (about 6–12 mixing volumes), and then purged for 12–24 h (about 0.7–1.3 mixing volumes) with air from a clean air generator. Before the injection of hydrocarbons and oxides of nitrogen (NO_x), an inert gas, sulfur hexafluoride (SF_6), was added to the chamber and was chromatographically separated and measured. The loss rate of SF_6 over the course of each experiment was used as the dilution rate in the model. Nitric oxide (NO) was added to the chamber first while internal chamber mixing fans were running. After the NO_x concentration was established, d-limonene and α-pinene were introduced into the chamber by vaporizing a measured amount of pure liquid (98%, Aldrich, Milwaukee, WI) in a U-tube that was gently heated by a hot air heat gun, and flushed by a dry nitrogen stream. After this point, chamber-mixing fans were turned off to reduce particle wall deposition. Gas-phase d-limonene and α-pinene concentration were measured every 10 min by gas chromatography. Chamber NO and total NO_x concentrations were monitored by a chemiluminescent nitrogen oxide analyzer. Ozone (O_3) was measured by a UV photometric ozone analyzer. These instruments were calibrated on each experiment via gas-phase titration using a US National Institute of Standards and Technology (NIST) traceable 51 ppm NO in a nitrogen tank. The temperature and humidity of the chamber were continuously monitored during the experiments and these values were used in the model simulations. Total solar and UV radiation were also measured continuously. Particle size distribution data (13–690 nm) were collected by a Scanning Mobility Particle Sizer (SMPS 3936 TSI, MN) composed of a Differential Mobility Analyzer (TSI long DMA, 3081, MN) and a Condensation Particle Counter (TSI CPC, 3022, MN).

3. Mechanism development

Individual UNC mechanisms for α-pinene and d-limonene are described elsewhere (Kamens et al., 1999; Kamens and Jaoui, 2001; Leungsakul et al., 2005a, b). Briefly, initial reactions of OH, O_3 and NO_3 with the terminal and internal double bonds of d-limonene or the double bond of α-pinene to form

C_{10}- and C_9-oxygenated products were called first-generation products. These first-generation products underwent further reactions in which the remaining double bond of d-limonene is oxidized by O_3, OH and NO_3 leading to second-generation products and these, in turn, underwent further oxidative steps leading to third-generation products. These second and third-generation products were, however, generalized according to their functional groups to reduce the number of species and reaction steps in the mechanism. For example, C_7-CHO represents all resulting C_8 aldehydes that do not contain a double bond. Rapid gas-particle equilibrium was assumed for organic products that appeared in both phases.

In the merged new mechanism, in view of the large number of organic peroxy radicals (RO_2) generated from the α-pinene and d-limonene, it was unrealistic to represent all the self-reactions and cross-reactions explicitly. An optimization technique to represent all of these reactions is needed. We have previously shown (Leungsakul et al., 2005b) that it was possible to group all of the RO_2 radicals into a total RO_2 scalar quantity and react that quantity with individual RO_2 radicals. In the present work, "TOT_RO_2" was defined, which was the sum of the concentration of all peroxy radicals. Each peroxy radical was assumed to react with all other peroxy radicals at a single collective rate (k_i). The use of a simplified parameterization was also essential, as discussed by Madronich and Calvert (1990):

$$RO_2 \rightarrow \gamma_1 RO + \gamma_2 R_{-H}O + \gamma_3 ROH, \quad k_i TOT\_RO_2 \tag{1}$$

where γ_1, γ_2 and γ_3 are the branching ratios which depend on the structure of the radical.

A thermal gas phase decomposition rate constant for acylperoxynitrates (Noziere and Barnes, 1998) of $10^{9.25} \times e^{-72/RT} s^{-1}$ was used, where R equals $8.314\,J\,K^{-1}\,mol^{-1}$, T is temperature in K, and the activation energy of 72 has units of $J\,mol^{-1}$. Partitioning rate coefficients for organic nitrates were estimated from calculations of the equilibrium portioning coefficient for a species i (^iK_p) as per Pankow (1994). ^iK_p was set equal to the rate coefficient describing semi-volatile particle up-take ($^ik_{on}$) divided by the rate coefficient for semi-volatile loss from the particles ($^ik_{off}$) (Kamens et al., 1999). Saturated liquid vapor pressure was used in the calculation of (^iK_p). For organic nitrates we used the estimation method of Nielsen et al. (1998) because vapor pressures of nitrates are higher than the values estimated from group contribution methods.

A kinetic approach that was used to represent the gas-particle partitioning processes (Kamens et al., 1999; Kamens and Jaoui, 2001) incorporates gas-particle partitioning with gas phase kinetics by explicitly expressing absorption and desorption of each semi-volatile partitioning species. To reduce the number of gas-particle partitioning cross-reaction steps, a scalar parameter "TOT_TSP" (similar to "TOT_RO_2") was introduced into the mechanism, which is the sum of all particle phase products and is computed at each time step. Instead of letting gas phase semi-volatile compounds explicitly partition onto each particle phase species, one pseudo first-order reaction was used to represent all these reactions with a rate coefficient of $k_{on} \times$ TOT_TSP:

$$SVC_{gas} \rightarrow SVC_{particle}, \quad k_{on} \times TOT\_TSP \tag{2}$$

In the new mechanism, a terminating C_8 stable oxygenated species (Stab-Oxy) produced from α-pinene reaction was updated to include subsequent reactions. Since our mechanism was linked to Carbon Bond 4 (CB4 2002) (Voicu, 2003; Whitten et al., 1980), Stab-Oxy was represented as paraffin (PAR) and XO_2 units, where XO_2 is a virtual radical that implicitly represents the oxidation of an RO_2 radical with NO, and the formation of NO_2. PAR and XO_2 then react within CB4 according to their specified CB4 reactions. Criegee reactions with water were changed to generate mostly pinonaldehyde, and cross-Criegee reactions (i.e. stabilized Creigee reactions with aldehydes, etc.) from both α-pinene and d-limonene were implemented. Exploratory oligomer reactions were included for α-pinene and d-limonene to represent ~35% of the particle mass as oligomers products as suggested by Gao et al. (2004a). Table 1 contains the simple oligomer reactions that we have included for α-pinene. Analogous reactions for limonaldehyde, and ketolimonaldehyde in the d-limonene system were also implemented. It was assumed that aldehyde–aldehyde particle phase dimerization reactions were faster then aldehyde–carboxylic acid.

There are many other possible particle phase reaction pathways in addition to the previously proposed reaction mechanisms of hydration, hemiacetal and acetal formation (Gao et al., 2004b; Jang et al., 2002; Kalberer et al., 2004; Tolocka et al.,

2004). At the present time we are not including oligomerization chemistry that requires a specific dependence on acidity. An exact representation of the combined mechanism is given in the supplemental material associated with this paper. To simulate each experiment we use the experimentally observed diurnal temperature, humidity and solar radiation profiles. The chemical mechanism however was "frozen" and remained constant (as is listed in the supplemental material) for all of the simulations. Hence all of the rate constants and all of the reactions are the same for each experiment, except for photoreactions (which depend on solar radiation), and temperature and pressure dependent reactions. The initial chamber conditions of each experiment were assessed from background analysis (such as background VOC concentration and aerosol concentration, which vary slightly from experiment to experiment). One of the most important factors is the initial HONO concentration. This varies from 0.02 to 2 ppb (in Table 2) and is used to improve the initial timing of each experiment. The amount that is added depends on the wall history of the experiments. If a high concentration experiment (0.3–5 ppm NO_x) preceded by a low concentration experiment, experience has shown that more wall HONO is available, even after venting the chamber and subsequent drying with air from a clean air generator.

Table 1
Oligomerization example reactions for α-pinene

	k_{rate} ($\times 10^{16}$ cm^3 molecule^{-1} s^{-1})
1. $pinald_p + pinald_p \rightarrow olig2$	7
2. $pinald_p + pinacid_p \rightarrow olig3$	1
3. $pinald_p + oxy\text{-}pinald_p \rightarrow olig4$	3
4. $pinald_p + oxy\text{-}pinacid_p \rightarrow olig5$	0.5
5. $pinald_p + diacid_p \rightarrow olig6$	0.1

Compound definitions for the particle phase are: $pinald_p$ is pinonaldehyde and norpinonaldehyde in the particle phase, pinacid is pinonic acid, diacid is pinic acid, oxypinald and acid are the sum of OH or carbonyl substituted pinonaldehyde and pinonic acid. Rates of reactions of particle phase aldehydes are assumed to be faster than aldehydes + acids although these compounds have been postulated. Similar reactions for oxypinonaldehydes and updates for limonaldehyde, and ketolimonaldehyde in the d-limonene system were also implemented.

4. Results and discussion

The initial conditions for all experiments are given in Table 2. SOA formation under two HC_0/NO_x conditions were studied: (1) high HC_0/NO_x experiments in which the initial HC_0/NO_x ranged from 1.60 to 2.92 and (2) low HC_0/NO_x experiments in which the initial HC_0/NO_x ranged from 0.60 to 0.95. The initial concentrations of d-limonene ranged from 0 to 260 ppbV, α-pinene from 0 to 980 ppbv, NO from 32 to 485 ppb, and NO_2 from 2 to 41 ppb. The temperature ranged from 280 to 315 K. All experiments were conducted under clear sunlight. The light intensity was converted to photons cm^{-2} s^{-1} at wavelengths that match absorption cross sections and quantum yields (Jeffries et al., 2003) for all photolysis species.

The time profile of the organic aerosol mass concentrations during photo-irradiation of α-pinene + d-limonene + NO_x-air systems is shown in Fig. 1. The aerosol mass concentrations (μg m^{-3}) were calculated from SMPS number distributions,

Table 2
Experimental conditions and initial concentrations

Experiment	Experiment date, MMDDYY	Initial concentration (ppbV)					Temperature (K)	Dewpoint (K)	HC_0/NO_x
		d-Limonene	α-Pinene	NO	NO_2	HONO[c]			
1	052504N[a]	260	0	65	24	0.01	298–313	287–290	2.92
2	052504S[a]	220	0	319	30	0.01	298–313	287–288	0.63
3	042006N[a]	25	50	89	18	1.50	280–307	277–279	0.70
4	042006S[a]	25	50	32	15	0.34	280–307	277–278	1.60
5	052406N[a]	42	97	106	41	2.00	277–306	272–273	0.95
6	103099[b]	0	940	485	2	1.28	300–308	277–282	1.93
7	060999[b]	0	980	430	2	0.20	295–315	281–286	2.27

[a]Performed in 270 m^3 dual chamber, N is the north chamber and S is the south chamber.
[b]Conducted in 190 m^3 chamber.
[c]HONO is not a measured quantity, but is adjusted to optimize model timing in the very initial part of the model simulation.

assuming a spherical particle shape and a density of 1.0–1.4 g cm^{-3}. The range bars in Fig. 1 were used to illustrate the values compared to a density of 1.2 g cm^{-3}. Aerosol mass concentrations from experiments from a previous α-pinene kinetic study in our 190 m^3 outdoor chamber (Kamens et al., 1999)

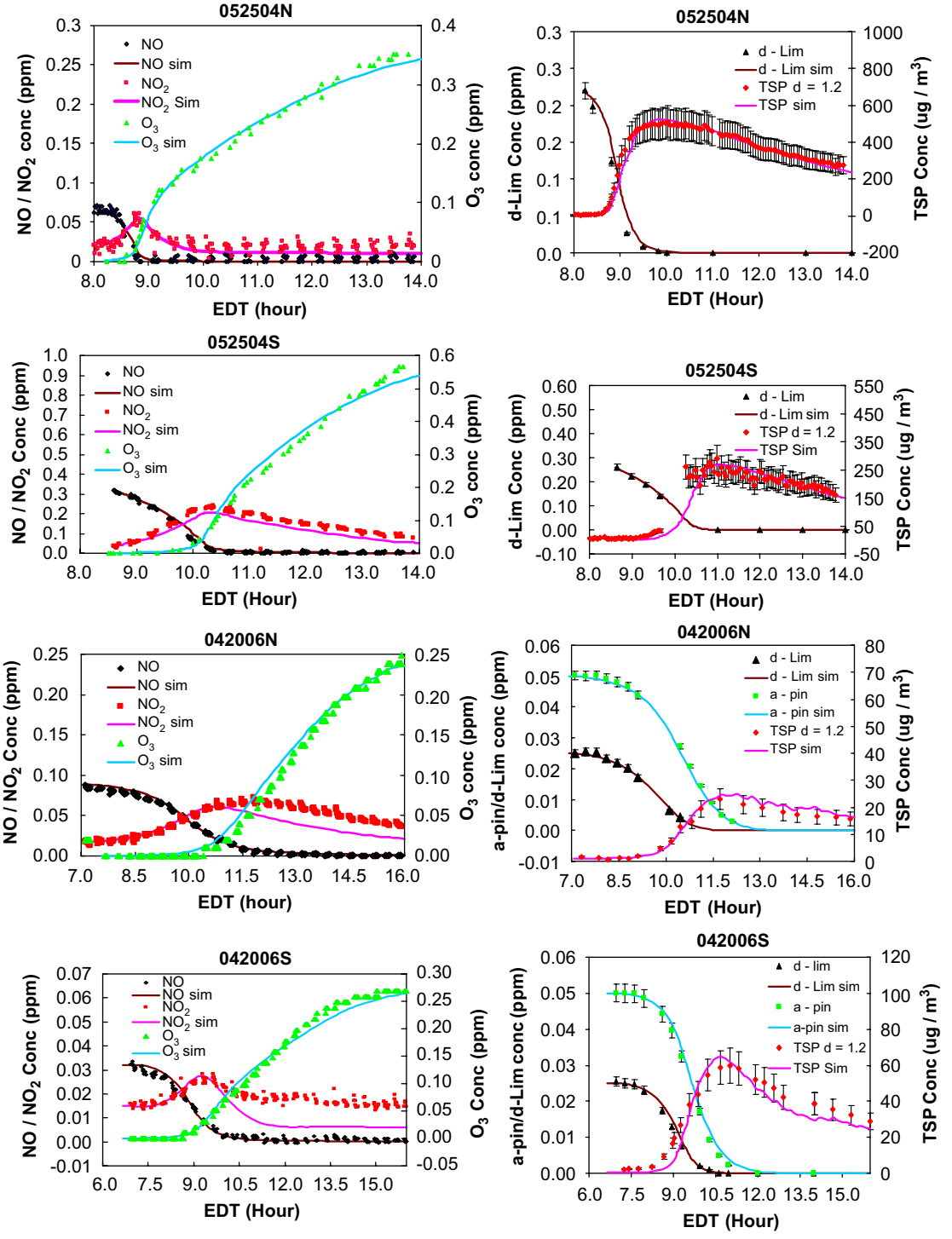

Fig. 1. Simulations of experimental data obtained from the UNC outdoor chamber facility, Pittsboro, NC. Data is represented by symbols, and model simulations are represented by solid lines unless otherwise specified.

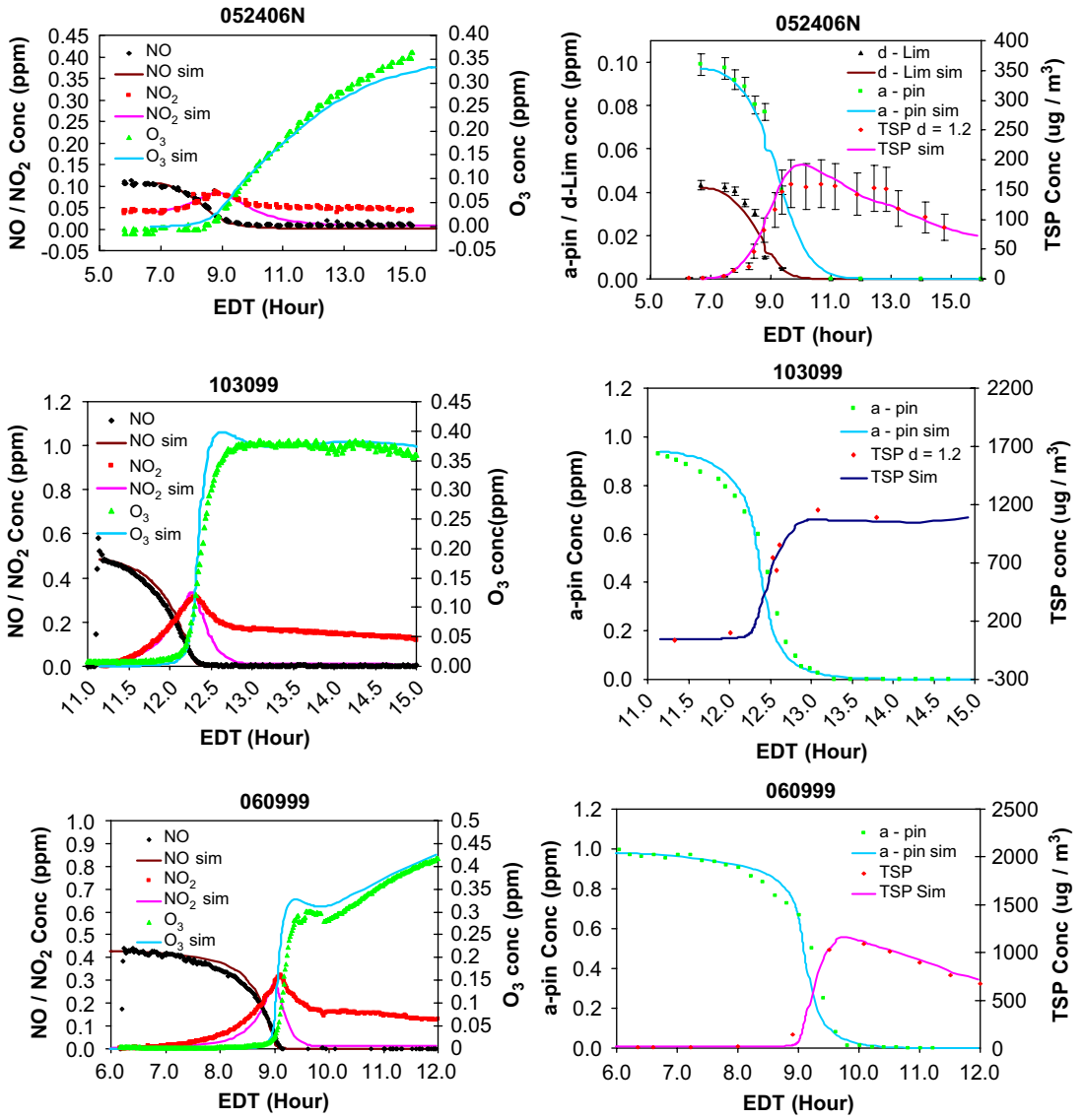

Fig. 1. (*Continued*)

with experiments that occurred on 9 June 1999 (060999) and 30 October 1999 (103099) were calculated from filter masses and sampling volumes. Time profiles for α-pinene, d-limonene, NO/NO_2 and O_3 are also plotted in Fig. 1; all are in units of ppmV. As shown in Fig. 1, there was a time delay between the onset of NO and α-pinene oxidation and SOA in most of our experiments. When NO approaches zero SOA growth commences. As NO approaches zero, the $RO_2 + HO_2$ reaction begins to compete with the $RO_2 + NO$ reaction and more nonvolatile products are formed in the gas and particle phases.

4.1. Combined model and simulations

Fig. 1 shows the model fits for the oxidation of α-pinene and d-limonene, O_3 and NO_x time–concentration profiles, and the model simulation concentration of SOA. The model closely simulates the behavior and timing for α-pinene, d-limonene, NO, NO_2, O_3 and SOA over a wide range of temperatures and concentrations. In experiments with mixtures of α-pinene and d-limonene, there was twice as much initial α-pinene compared to d-limonene, yet d-limonene accounted for 50–70% of the aerosol formation.

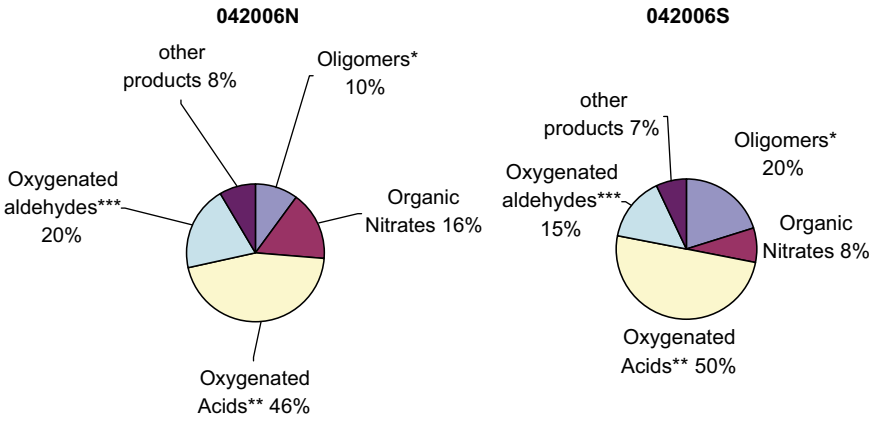

Fig. 2. Aerosol composition (% of mass) under different initial reactant concentrations. (*) Oligomers: seed1 was included, and is the "dimer" reaction product of C10 stabilized Criegee Biradicals with large aldehydes or carboxylic acid products. (**) Oxygenated acid: compounds with one or more –COOH groups (such as diacids). (***) Oxygenated aldehydes: hydroxypinonaldehydes, ketopinoladehydes, ketolimonaldehyde, etc.

A product comparison of different experiments (042006N with 042006S, see Table 2) in Fig. 2, showed that the experiment (042006N) with lower initial α-pinene and d-limonene to NO_x ratio (HC_0/NO_x) had ~10% oligomers in the particle phase. The 042006S with higher initial HC_0/NO_x had ~20% oligomers in particle phase. This suggests that the relative importance of oligomers (polymer) varies with different conditions.

4.2. Factors affecting SOA–NO_x–VOC sensitivity

To further our understanding of the different factors that influence SOA formation, a sensitivity analysis was first undertaken by using a factorial design. Over 100 simulations were performed at different conditions. We found that the order of the most important factors that influenced SOA was: percentage of d-limonene in the mixture > hydrocarbon to NO_x ratio > temperature > light intensity.

4.2.1. Percentage of d-limonene on SOA yield

The model responses (Fig. 3) to the changes of the percentages of d-limonene in the 0.10 ppmV mixture of d-limonene and α-pinene were further evaluated at seven different ratios with a constant NO_x level and environmental conditions similar to the 24 May 2006 (052406) experiment as noted in Table 2. Yield was defined as the maximum SOA formed divided by the amount of hydrocarbon reacted (SOA $\mu g\,m^{-3}$)/(ΔHC $\mu g\,m^{-3}$). A plot (Fig. 3b) of the aerosol yield as a function of the percentage of d-limonene suggested that higher d-limonene fractions of the total α-pinene and d-limonene mixture led to higher aerosol yields. A polynomial fit to the yield vs. the fraction of d-limonene in the mixture gave

$$Y_{SOA} = 2 \times 10^{-5} X^2 + 0.0032X + 0.0562, \quad R^2 = 0.999, \tag{3}$$

where Y_{SOA} is the aerosol yield, and X is the percentage of d-limonene in the 0.10 ppm mixture of d-limonene and α-pinene. Although the coefficients represented specifically the environmental conditions of the 052406 experiment, the characteristic shape applies to other environmental conditions with α-pinene/d-limonene mixtures. At other HC/NO_x ratios and experiment conditions (temperature, sun light, dew point), we also observed this near-linear behavior, but the coefficients are environmentally dependent.

4.2.2. Impact of hydrocarbon to NO_x ratios (HC_0/NO_x)

The HC_0/NO_x ratio has a potentially large impact on SOA production (Kroll et al., 2006). In this work, the model response to the changes in the HC_0/NOx ratio (Fig. 4) was evaluated at seven different levels (NO_x was varied with HC_0 held constant) with a constant α-pinene/d-limonene ratio (0.05/0.05, ppmV/ppmV), and environmental conditions similar to the 052406 experiment as shown in Table 2. In general, increasing the HC_0/NO_x ratio increased the SOA yield up to a ratio <2.5. Above this point, increasing the HC_0/NO_x ratio decreased

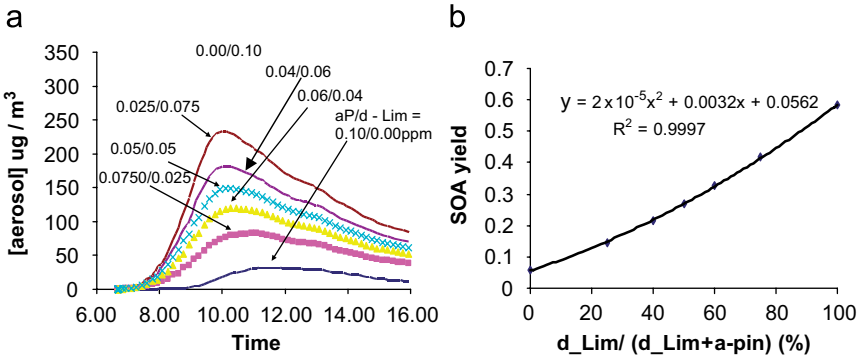

Fig. 3. Evaluation of the effect of the percentage of d-limonene on SOA yield.

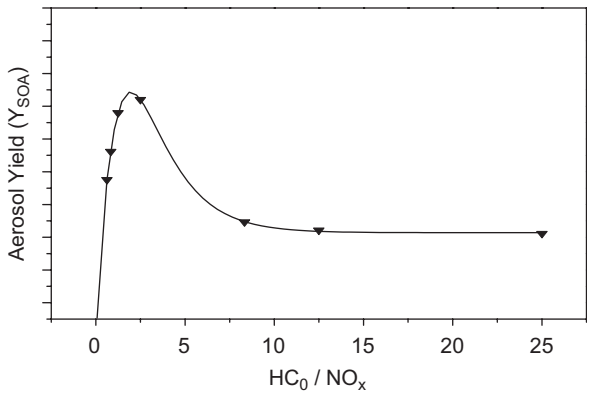

Fig. 4. Aerosol yields as functions of hydrocarbon to NO_x ratio. The symbols (▼) were kinetic model data simulated from a constant α-pinene/d-limonene ratio (0.05/0.05, ppmV/ppmV), and similar environmental conditions to the 24 May 2006 in Table 2. The solid line was pulse function fit (Eq. (4)).

SOA yields. Different statistical forms were used to predict the yield of SOA as a function of just the HC_0/NO_x ratio. We observed that a pulse function gave the best fit of these data:

$$Y_{SOA} = 0.157 + 1.06(1 - e^{-((X-0.218)/1.82)})^{1.47} \times e^{-((X-0.218)/1.97)}, \quad R^2 = 0.999, \qquad (4)$$

where Y_{sos} is SOA yield and X is HC_0/NO_x.

Previous studies (Poppe et al., 1993) have shown that the OH concentration for fixed hydrocarbon concentrations was governed by the NO_x mixing ratio. The OH radical concentrations tended to be high at low NO_x levels and were inhibited at high NO_x levels. This was the same trend that we observed for the impact of the HC_0/NO_x ratio on SOA formation, and this coincidence implied that OH radical chemistry impacted SOA yields to a greater extent than other reactions.

4.2.3. Impact of temperature on SOA

The model response to changes in temperature was evaluated with different HC_0/NO_x ratio conditions (similar to the 042006 experiment in Table 2). In the high HC_0/NO_x ratio simulation (1.60), when temperature increased 10 K, SOA yield (Y_{SOA}, TSP = 64.8 μg m^{-3}) decreased 56%; and when temperature decreased 10 K, Y_{SOA} increased +60%. With the low HC_0/NO_x ratio (0.70), when the temperature increased 10 K, Y_{SOA} (TSP = 25 μg m^{-3}) decreased by 75%; when the temperature decreased 10 K, Y_{SOA} increased by 96%. The greater impact of temperature on SOA at the low HC_0/NO_x ratio (0.70) than with the high ratio (1.6) was due to a relatively higher percentage of organic nitrates generated under the low HC_0/NO_x ratio (0.70) conditions. With high levels of NO_x (low HC_0/NO_x ratios), the reactions of radicals with NO_x increase in importance, leading to nitrogen-containing products such as pinonaldehyde PAN (pinald-PAN), hydroxy α-pinene nitrates (HO-apNO3), internal hydroxy-d-limonene nitrates (hyd lim-OH-*i*ONO2), and external hydroxy d-limonene nitrates (lim-OH-*x*ONO2). Higher percentages of organic nitrates will result in a higher temperature dependence of SOA yields because: (1) organic nitrates compounds have higher vapor pressures than oxygenated analogues; (2) the thermal decomposition reactions of acylperoxy organic nitrates are very temperature sensitive (such PAN, and α-pinene and d-limonene derived PAN type compounds); and (3) recent work has implicated the production of high molecular weight compounds by heterogeneous particle reactions

(Jang et al., 2002; Tolocka et al., 2004) between different function groups: carboxylic acids (–C(=O)OH), aldehydes (–C(=O)H), ketones (–C(=O)–) and alcohols (–OH). This acts as a driving force for SOA formation and growth. As oligomers are formed, the temperature dependence of SOA formation decreases because of the very low volatility of the oligomer fraction.

5. An atmospheric example

By modifying inputs to the model to include diurnal emissions, changing mixing heights and deposition rates specific to a forest canopy, we attempted to simulate remote atmospheric SOA conditions that might result from realistic emissions of α-pinene, d-limonene and NO_x.

Since monoterpenes are stored in resin ducts of needles, their emission rate depends on osmosis/evaporation from these storage pools (Dement et al., 1975; Tingey et al., 1980). The rate of monoterpene emissions is found to increase exponentially with temperature (Schuh et al., 1997):

$$\phi_{\mathrm{voc}} = \phi^{\mathrm{s}}_{\mathrm{voc}} \exp\left[\frac{C_{\mathrm{tp}}}{R}\left(\frac{T - T_{\mathrm{s}}}{TT_{\mathrm{s}}}\right)\right],$$

where ϕ_{voc} is the VOC emission rate, $\phi^{\mathrm{s}}_{\mathrm{VOC}}$ is the VOC emission rate under standard conditions, R is the gas constant, T is the temperature, T_{s} is the standard temperature (298 K), and C_{tp} is an empirical parameter describing the temperature dependence of emissions.

The emission rates of α-pinene and d-limonene for our simulations are shown in Fig. 5a. These processes were represented as first-order reactions with corresponding temperature dependent rate coefficients:

$$\Longrightarrow \alpha\text{-pinene} \quad k_{\alpha\text{-P\_Emission}},$$
$$\Longrightarrow \text{d-limonene} \quad k_{\text{d Lim\_Emission}},$$

where $k_{\alpha\text{-P\_Emission}} = 3.0 \times 10^6 \times e^{(33.2(T-298)/T)}$ molecules $\mathrm{cm^{-3}\,s^{-1}}$ and $k_{\text{d Lim\_Emission}} = 1.0 \times 10^6 \times e^{(33.2(T-298)/T)}$. They were used to describe emission rates by taking related parameters (Komenda and Koppmann, 2002), and assuming a needle density ($7.41 \times 10^{-7}\,\mathrm{g\,cm^{-3}}$). We also assumed that the overall emission rate coefficient of d-limonene is ~1/3 of that of total α- and β-pinene (Griffin et al., 1999).

In remote and rural areas, NO_x budgets are controlled by soil NO emissions, and estimates of the soil NO sources range between 9.7 TgN $\mathrm{yr^{-1}}$ (Potter et al., 1996) and 21 TgN $\mathrm{yr^{-1}}$ (Davidson and Kingerlee, 1997). The production of soil NO is mainly controlled by soil environmental conditions such as soil-temperature, moisture, fertility, vegetation cover, fire and land use management (Valente and Thornton, 1993; Williams and Fehsenfeld, 1991). In this study, the rate of NO_x emissions was assumed to increase linearly with temperature; the fraction of NO_2 was 30% as per Lenner (1987):

$$\Longrightarrow \mathrm{NO} \quad k_{\mathrm{NO\ Emission}},$$
$$\Longrightarrow \mathrm{NO_2} \quad k_{\mathrm{NO_2\ Emission}},$$

where $k_{\mathrm{NO\ Emission}} = 3 \times k_{\mathrm{NO_2\ Emission}} = 2.0 \times 10^6 \times T/298$ molecules $\mathrm{cm^{-3}} s^{-1}$.

To initiate the model simulation, the following initial ppbV concentrations were used: 0.2 NO, 0.1 NO_2, 0.3 α-pinene, and 0.1 limonene, and this is consistent with observed levels in remote environments (Das and Aneja, 2003). The temperature, humidity, and natural sunlight were all similar to the 24–25 May 2006 experiments. The physical removal was also considered in our simulation, which was included in mixing height changes and the deposition to surfaces. As an approximation, the mixing height change was implemented as a variable dilution rate 0.01–0.10 $\mathrm{h^{-1}}$ (Fig. 5b), and the half-life ($T_{1/2}$) of particle deposition was assumed to be 4 days. A two-day simulation results are shown in Fig. 5b. O_3 concentrations reached a maximum of 43 ppb on the first day and 44 ppb on the second day. With temperature dependent NO_x, α-pinene and d-limonene emissions, the aerosol concentration increased steadily and reached its maximum value 1.5 $\mu\mathrm{g\,m^{-3}}$ on the first day and then it slowly decreased at night. On the second day, aerosol concentrations began to increase after sunrise to a maximum value of 3.0 $\mu\mathrm{g\,m^{-3}}$. On average, α-pinene accounted for 10–20% of the aerosol formation.

Over a Eucalyptus forest in Portugal, Kavouras et al. (1999) measure ~0.25 $\mu\mathrm{g\,m^{-3}}$ of α-pinene particle phase SOA oxidation products (*cis*- and *trans*-pinonic, norpinonic and pinic acids). They do not report oxygenated pinonic aldehydes and pinonic acids, and associated α-pinene nitrated product acids. They also do not report on d-limonene SOA products, but since the ratio of our concentrations products is three times more SOA from d-limonene than α-pinene, one might expect 1.5–2 $\mu\mathrm{g\,m^{-3}}$ of SOA from such a system.

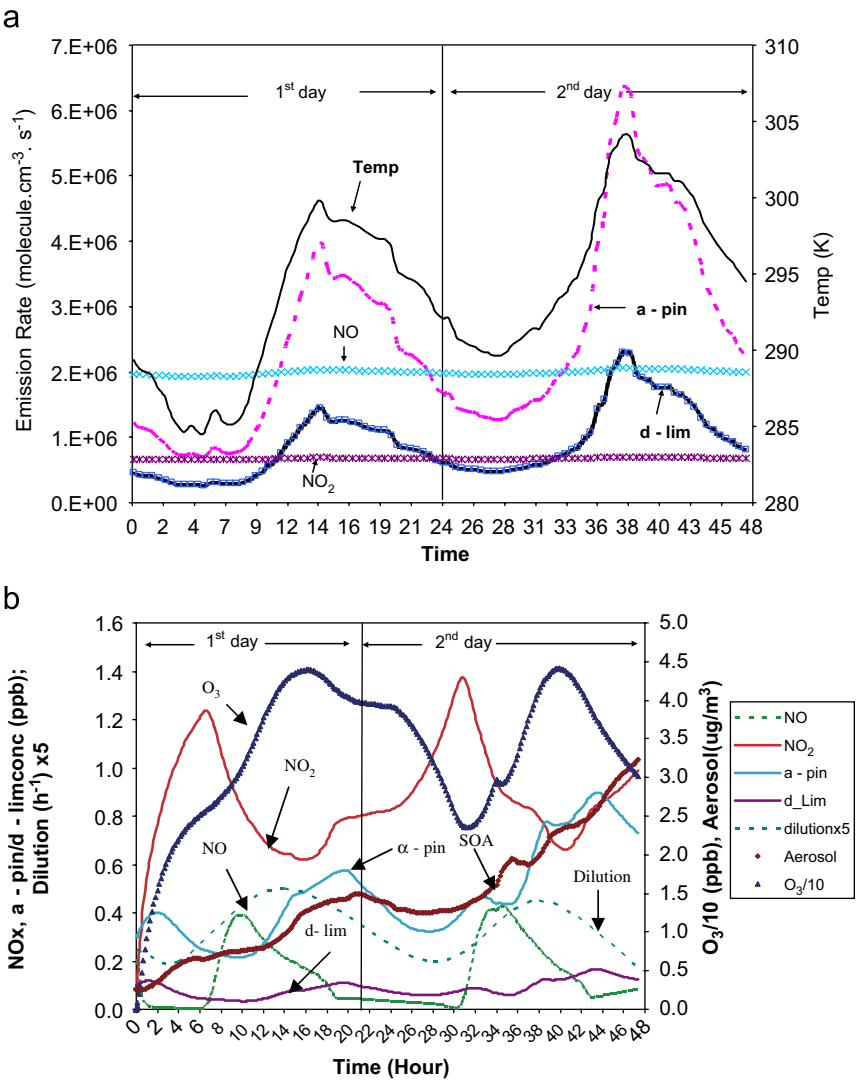

Fig. 5. (a) α-pinene, d-limonene, and NO_x emission rates, expressed as a product of a temperature dependent term. (b) α-pinene and d-limonene photo-oxidation simulation with NO_x, α-pinene and d-limonene emissions.

Olszyna et al. (2005) reported a $PM_{2.5}$ mass concentration 13.3–33.7 $\mu g\,m^{-3}$ in the Great Smoky Mountains National Park; 30–50% of this is sulfate. If only 10% of the remainder is organic (a low estimate) and 30–80% of this is SOA from terpenes, one estimates terpenene SOA concentrations of 0.3–1 $\mu g\,m^{-3}$. Given the above, a model system that generates 3 $\mu g\,m^{-3}$ does not seem unreasonable if one assumes that α-pinene and d-limonene are surrogates for the entire terpene system.

The predicted oligomer contribution to the aerosol mass increased with time. In the morning hours (0:00 midnight to 09:00 a.m.) on the first day, particle phase reactions that produced oligomers accounted for ~5% of the aerosol mass. At 5:00 p.m. on the first day, these reactions accounted for ~15%; this increased to ~25% in the morning on the second day, and reached a maximum of ~30% during the daytime of the second day. This suggests that the volatility of the simulated SOA material on the aging aerosol was decreasing with time, which is consistent with chamber observations (Kalberer et al., 2004). Of additional importance is that our simulation does not show a loss of SOA during the daytime and this is consistent with observed measurements (Kleeman and Ying, 2006). When our original α-pinene mechanism was conceived (Kamens et al., 1999; Kamens and Jaoui,

2001), it did not include oligomerization reactions. In the new α-pinene portion of the mechanism, we included particle phase dimerization reactions that account for as much as ~35% of the SOA mass. The d-limonene mechanism shunted ~20% of the mass into oligomer products, when stabilized Criegee + carboxylic acid products were considered. If oligomers were not included, as in the original α-pinene mechanism, we do not see a significant effect on first day SOA formation. Under a two or three day simulation, however, without oligomerization reactions, SOA decreases as the diurnal temperature increases. We have called this artifact an "inverse belly" effect. If oligomers are included we do not observe this phenomenon, and this is agreement with real observations. Confirmation of these simulated observations, however, awaits detailed measurements of oligomers in the atmosphere and corresponding low-concentration chamber experiments.

Acknowledgments

This work is supported by a STAR grant from the US EPA (RD-83108401) to the University of North Carolina at Chapel Hill. Sincere thanks to Professor Harvey Jeffries for the Allomorphic Mechanism Software.

Appendix A. Supplementary materials

Supplementary data associated with this article can be found in the online version at doi:10.1016/j.atmosenv.2007.09.017.

References

Das, M., Aneja, V.P., 2003. Regional analysis of nonmethane volatile organic compounds in the lower troposphere of the southeast United States. Journal of Environmental Engineering 129 (12), 1085–1103.

Davidson, E.A., Kingerlee, W., 1997. A global inventory of nitric oxide emissions from soils. Nutrient Cycling in Agroecosystems 48 (1–2), 37–50.

Dechapanya, W., Eusebi, A., Kimura, Y., Allen, D.T., 2003. Secondary organic aerosol formation from aromatic precursors. 1. Mechanisms for individual hydrocarbons. Environmental Science and Technology 37, 3662–3670.

Dement, W., Tyson, B., Mooney, H., 1975. Mechanism of monoterpene volatilization in *Salvia mellifera*. Phytochemistry 14, 2555–2557.

Gao, S., Keywood, M., Ng, N.L., Surratt, J., Varutbangkul, V., Bahreini, R., Flagan, R.C., Seinfeld, J.H., 2004a. Low-molecular-weight and oligomeric components in secondary organic aerosol from the ozonolysis of cycloalkenes and α-pinene. Journal of Physical and Chemistry A 108, 10147–10164.

Gao, S., NG, N.A., Keywood, M., Varutbangkul, V., Bahreini, R., Nenes, A., He, J., Yoo, K.Y., Beauchamp, J.L., Hodyss, R.P., Flagan, R.C., Seinfeld, J.H., 2004b. Particle phase acidity and oligomer formation in secondary organic aerosol. Environmental Science and Technology 38 (24), 6582–6589.

Griffin, R.J., Cocker III, D.R., Seinfeld, J.H., Dabdub, D., 1999. Estimate of global atmospheric organic aerosol from oxidation of biogenic hydrocarbons. Geophysical Research Letters 26 (17), 2721–2724.

Jang, M., Czoschke, N.M., Lee, S., Kamens, R.M., 2002. Heterogeneous atmospheric aerosol production by acid-catalyzed particle-phase reactions. Science 298 (5594), 814–817.

Jeffries, H.E., Kessler, M., Gery, M., 2003. Mcomp/meval: the morphecule photochemical reaction mechanism. 〈http://airchem.sph-unc/Research/Products/Software/Morpho/docs.html〉.

Kalberer, M., Paulsen, D., Sax, M., Steinbacher, M., Dommen, J., Prevot, A.S.H., Fisseha, R., Weingartner, E., Frankevich, V., Zenobi, R., Baltensperger, U., 2004. Identification of polymers as major components of atmospheric organic aerosols. Science 303 (5664), 1659–1662.

Kamens, R.M., Jaoui, M., 2001. Modeling aerosol formation from α-pinene + NO_x in the presence of natural sunlight using gas-phase kinetics and gas-particle partitioning theory. Environmental Science and Technology 35, 1394–1405.

Kamens, R., Jang, M., Chien, C.-J., Leach, K., 1999. Aerosol formation from the reaction of α-pinene and ozone using a gas-phase kinetics-aerosol partitioning model. Environmental Science and Technology 33, 1430–1438.

Kavouras, I.G., Mihalopoulos, N., Stephanou, E.G., 1999. Secondary organic aerosol formation vs primary organic aerosol emission: in situ evidence for the chemical coupling between monoterpene acidic photooxidation products and new particle formation over forests. Environmental Science and Technology 33 (7), 1028–1037.

Kleeman, M., Ying, Q., 2006. Source apportionment of secondary air pollutants. In: International Conference on Atmospheric Chemical Mechanisms.

Komenda, M., Koppmann, R., 2002. Monoterpene emissions from scots pine (*pinus sylvestris*): field studies of emission rate variabilities. Journal of Geophysical Research 107, 4161–4174.

Kroll, J.H., Ng, N.L., Murphy, S.M., Flagan, R.C., Seinfeld, J.H., 2006. Secondary organic aerosol formation from isoprene photooxidation. Environmental Science and Technology 40, 1869–1877.

Lee, S., Jang, M., Kamens, R.M., 2004. SOA formation from the photooxidation of α-pinene in the presence of freshly emitted diesel soot exhaust. Atmospheric Environment 38, 2597–2605.

Lenner, M., 1987. Nitrogen dioxide in exhaust emission from motor vehicles. Atmospheric Environment 21, 37–43.

Leungsakul, S., Jaoui, M., Kamens, R.M., 2005a. Kinetic mechanism for predicting secondary organic aerosol formation from the reaction of d-limonene with ozone. Environmental Science and Technology 39 (24), 9583–9594.

Leungsakul, S., Jeffries, H.E., Kamens, R.M., 2005b. A kinetic mechanism for predicting secondary aerosol formation from

the reaction of d-limonene in the presence of oxides of nitrogen and natural sunlight. Atmospheric Environment 39, 7063–7082.

Liggio, J., Li, S.-M., McLaren, R., 2005a. Heterogeneous reactions of glyoxal on particulate matter: identification of acetals and sulfate esters. Environmental Science and Technology 39 (6), 1532–1541.

Liggio, J., Li, S.-M., McLaren, R., 2005b. Reactive uptake of glyoxal by particulate matter. Journal of Geophysical Research 110, D10304.

Madronich, S., Calvert, J.G., 1990. Permutation reactions of organic peroxy radical in the troposphere. Journal of Geophysical Research 95, 5697–5715.

Nielsen, T., Platz, T., Granby, K., Hansen, A.B., Skov, H., Egelov, A.H., 1998. Particulate organic nitrates: sampling and night/day variation. Atmospheric Environment 32, 2601–2608.

Noziere, B., Barnes, I., 1998. Evidence for formation of a pan analog of pinonic structure and investigation of its thermal stability. Journal of Geophysical Research (Atmospheres) 103, 25587–25597.

Odum, J.R., Hoffmann, T., Bowman, F., Collins, D., Flagan, R.C., Seinfeld, J.H., 1996. Gas/particle partitioning and secondary organic yields. Environmental Science and Technology 30, 2580–2585.

Olszyna, K.J., Bairai, S.T., Tanner, R.L., 2005. Effect of ambient NH_3 levels on pm 2.5 composition in the Great Smoky Mountains National Park. Atmospheric Environment 39 (25), 4593–4606.

Pankow, J.F., 1994. An absorption model of the gas/aerosol partitioning involved in the formation of secondary organic aerosol. Atmospheric Environment 28, 189–193.

Poppe, D., Wallasch, M., Zimmermann, J., 1993. The dependence of the concentration of OH on its precursors under moderately polluted conditions: a model study. Journal of Atmosphere Chemistry 16, 61–78.

Potter, C.S., Matson, P.A., Vitousek, P.M., Davidson, E.A., 1996. Process modeling of controls on nitrogen trace gas emissions from soils worldwide. Journal of Geophysical Research-Atmospheres 101 (D1), 1361–1377.

Schuh, G., Heiden, A.C., Hoffmann, T., Kahl, J., Rockel, P., Rudolph, J., Wildt, J., 1997. Emissions of volatile organic compounds from sunflower and beech: dependence on temperature and light intensity. Journal of Atmosphere Chemistry 27, 297–318.

Takekawa, H., Minoura, H., Yamazaki, S., 2003. Temperature dependence of secondary organic aerosol formation by photo-oxidation of hydrocarbons. Atmospheric Environment 37, 3412–3424.

Tingey, D.T., Manning, M., Grothaus, L.C., Burns, W.F., 1980. Influence of light and temperature on monoterpene emission rates from slash pine. Plant Physiology 65, 797–801.

Tolocka, M.P., Jang, M., Ginter, J.M., Cox, F.J., Kamens, R.M., Johnston, M.V., 2004. Formation of oligomers in secondary organic aerosol. Environmental Science and Technology 38 (5), 1428–1434.

Valente, R.J., Thornton, F.C., 1993. Emissions of NO from soil at a rural site in Central Tennessee. Journal of Geophysical Research-Atmospheres 98 (D9), 16745–16753.

Voicu, I., 2003. A Revised Carbon Bond Mechanism. Department of Environmental Sciences and Engineering.

Whitten, G.Z., Hogo, H., Killus, J., 1980. The Carbon-Bond mechanism: a condensed kinetic mechanism for photochemical smog. Environmental Sciences and Technology 14 (6), 690–700.

Williams, E.J., Fehsenfeld, F.C., 1991. Measurement of soil-nitrogen oxide emissions at 3 north-american ecosystems. Journal of Geophysical Research-Atmospheres 96 (D1), 1033–1042.